

The spectral energy distribution of PKS 2004–447: a compact steep-spectrum source and possible radio-loud narrow-line Seyfert 1 galaxy

L. C. Gallo,^{1,2} P. G. Edwards,² E. Ferrero,³ J. Kataoka,⁴ D. R. Lewis,^{5,6} S. P. Ellingsen,⁶ Z. Misanovic,¹ W. F. Welsh,⁷ M. Whiting,⁵ Th. Boller,¹ W. Brinkmann,¹ J. Greenhill⁶ and A. Oshlack^{8,9}

¹ Max-Planck-Institut für extraterrestrische Physik, Postfach 1312, 85741 Garching, Germany

² Institute of Space and Astronautical Science, Japan Aerospace Exploration Agency, 3-1-1 Yoshinodai, Sagamihara, Kanagawa 229-8510, Japan

³ Landessternwarte Heidelberg, Königstuhl 12, D-69117, Heidelberg, Germany

⁴ Department of Physics, Tokyo Institute of Technology, 2-12-1 Ohokayama, Meguro, Tokyo 152-8551, Japan

⁵ Australia Telescope National Facility, CSIRO, PO Box 76, Epping, NSW 1710, Australia

⁶ School of Mathematics and Physics, University of Tasmania, Private Bag 37, Hobart, TAS 7001, Australia

⁷ Department of Astronomy, San Diego State University, San Diego, CA 92182, USA

⁸ School of Physics, University of Melbourne, Parkville VIC 3010, Australia

⁹ current address: Bioinformatics Division, Walter and Eliza Hall Institute of Medical Research, Parkville VIC 3050, Australia

Accepted. Received.

ABSTRACT

An investigation of the spectral energy distribution (SED) of the compact steep-spectrum (CSS) source and possible radio-loud narrow-line Seyfert 1 galaxy (NLS1), PKS 2004–447, is presented. Five out of six well-studied radio-loud NLS1 share this dual classification (optically defined as a NLS1 with radio definition of a CSS or giga-hertz peaked spectrum (GPS) source), suggesting that the connection could have a physical origin. The SED is created from simultaneous observations (within 24 hours) at radio (from ATCA), optical/NIR (from Siding Spring) and UV/X-ray (from *XMM-Newton*) wavelengths. The X-ray data show evidence of short-term variability (primarily a ~ 30 per cent increase in the final 4 ks of the observation), a possible soft excess, and negligible absorption. Together with the rest of the SED, the X-ray emission is excessive in comparison to synchrotron plus synchrotron self-Compton (SSC) models. The SED can be described with a two component model consisting of extended synchrotron/SSC emission with Comptonisation in the X-rays, though SSC models with a very high electron-to-magnetic energy density ratio cannot be excluded either. The peak emission in the SED appears to be in the near infrared, which can be attributed to thermal emission ($T \approx 1000$ K) from a dusty torus. Analysis of a non-contemporaneous, low-resolution optical spectrum suggests that the narrow-line region (NLR) is much more reddened than the X-ray emitting region suggesting that the gas-to-dust ratio in PKS 2004–447 may be very different than in our own Galaxy. This could be achieved if the radio jets in PKS 2004–447 deposits material from the nucleus into the NLR. Long-term radio monitoring of PKS 2004–447 shows a rather constant light curve over nearly a six month period with the exception of one outburst when the 6.65 GHz flux increased by ~ 35 per cent over 19 days. It is not possible to differentiate between intrinsic or extrinsic (i.e., interstellar scintillation) origins for this outburst, but the detection of the rare event demonstrates the importance of intensive monitoring campaigns. In comparison to general samples of GPS sources, which appear to be X-ray weak, NLS1-CSS/GPS sources possess stronger X-ray emission relative to radio (comparable to normal radio-loud AGN). In addition, NLS1-CSS/GPS sources also exhibit lower intrinsic absorption than GPS sources of similar X-ray luminosity. This is consistent with the additional X-ray component required for PKS 2004–447, but larger samples of NLS1-CSS/GPS are needed before any conclusive remarks can be made.

Key words: galaxies: active – galaxies: nuclei – quasars: individual: PKS 2004–447 – radio continuum: galaxies – X-ray: galaxies

1 INTRODUCTION

Compact steep-spectrum (CSS) and giga-hertz peaked spectrum (GPS) sources constitute a large fraction of the powerful ($\log P_{1.4} \gtrsim 25 \text{ W Hz}^{-1}$) radio source population. Morphologically, they are compact and often only partially resolved on milliarcsecond scales, with projected linear sizes of less than 1 and 20 kpc for GPS and CSS, respectively. However, these objects are not just radio cores, rather they constitute complete systems with small-scale jets and lobes.

Two scenarios have been proposed that attempt to explain the CSS/GPS phenomenon (see O’Dea 1998 for a review). The first is that CSS/GPS sources form stages of an evolutionary sequence for all large radio sources. The more compact objects (GPS) are the youngest sources which, with time, expand in size to form CSS and eventually large radio objects (the youth scenario). The second picture is that CSS/GPS sources are kept compact by high density material which inhibits the radio source from expanding (frustrated scenario).

The radio spectra of GPS sources show curvature with peaks above 500 MHz. CSS objects are characterised by steep spectra ($\alpha > 0.5$; $S \propto \nu^{-\alpha}$) with a low-frequency, often undetectable, turnover (e.g. $\nu_t \approx 100 \text{ Hz}$). Perhaps the strongest evidence linking GPS and CSS sources is the relationship (anticorrelation) between turnover frequency and projected linear size (Fanti et al. 1990; O’Dea & Baum 1997). In fact, it has been suggested that GPS sources evolve into CSS sources, and perhaps eventually into FR-I/II objects in a self-similar manner (Snellen et al. 2003).

Studies of the class properties of CSS/GPS quasars at other wavebands are less complete, but to first-order the observations are not radically different from non-CSS, radio-loud quasars. The far-infrared *IRAS* luminosities are consistent with arising from AGN, similar to extended, radio-loud quasars (e.g. Heckman et al. 1994). There is some evidence for an additional component in the near-infrared (NIR), which could be due to emission from $\sim 1000 \text{ K}$ dust, possibly from an AGN heated torus (de Vries et al. 1998). Host galaxies are comparable between GPS, CSS, and FR-II (e.g. de Vries et al. 2000). Optical spectra are rich in emission lines, similar to extended radio sources (e.g. Morganti et al. 1997) and the emission is aligned with the radio source suggesting interaction of the two mediums (e.g. the radio source shocks the emission-line gas) in the production of lines (e.g. Gelderman & Whittle 1994; de Vries et al. 1998; Bicknell et al. 1997; Labiano et al. 2005). Until recently there has been little focus on X-ray studies of CSS/GPS sources, primarily because they appear to be X-ray dim (Baker et al. 1995). This could be because of additional X-ray absorption, which has been detected in many objects of this class (e.g. Elvis et al. 1994; Guainazzi et al. 2006; Vink et al. 2006). Recent studies with *Chandra* and *XMM-Newton* show that the X-ray spectra of GPS source are well characterised by a single power law modified by intrinsic absorption (Guainazzi et al. 2006; Vink et al. 2006). X-ray variability on hourly time scales has only been reported for one GPS, COINS J0029 + 3456 (Guainazzi et al. 2006).

In this work we examine the spectral energy distribution (SED) of one CSS source, PKS 2004–447. The PKSCAT90 catalog (Wright & Otrupcek 1990) gives flux density measurements at frequencies between 408 MHz and 8.4 GHz for PKS 2004–447. These were not contemporaneous, but suggest that the slope of the radio spectrum is ~ 0.1 at low frequencies, steepening to > 0.5 at higher frequencies.

PKS 2004–447 also shows evidence for having an angular size of $< 1''$, as observations on the 6 km baseline of the Australia Tele-

scope Compact Array (ATCA) have revealed that ~ 99 per cent of the flux density is unresolved at 8.6 GHz (Lovell 1997; Tasker 2000). The source is partially resolved on longer baselines – on the 275 km Parkes–Tidbinbilla Interferometer baseline a correlated flux density at 2.3 GHz of 0.39 Jy was measured, in comparison to a contemporaneous total flux density of 0.68 Jy. However, the 2.3 GHz single-baseline VLBI survey of Preston et al. (1985) yielded a correlated flux density of $0.28 \pm 0.02 \text{ Jy}$ on a 10,000 km baseline, indicating the presence of a compact, parsec-scale core. The steep spectrum at cm wavelengths and sub-arcsecond structure match the criteria for CSS sources (Fanti et al. 1990).

A comparison of all reported flux density measurements for the source indicates that the source displays variability of ~ 20 per cent on the timescale of years at cm wavelengths. Moderate slow variability of CSS sources is not uncommon at these frequencies (e.g., Edwards & Tingay 2004).

PKS 2004–447 has encountered controversy (Oshlack et al. 2001, hereafter Osh01; Zhou et al. 2003; Sulentic et al. 2003) with its optical definition as a narrow-line Seyfert 1 galaxy (NLS1). By optical definition, NLS1 have narrow permitted lines ($\text{FWHM}(\text{H}\beta) \leq 2000 \text{ km s}^{-1}$), weak [O III] ($\frac{[\text{O III}]}{\text{H}\beta} < 3$), and strong Fe II (see Osterbrock & Pogge 1985 and Goodrich 1989). PKS 2004–447 satisfies the first two criteria, but has weak Fe II (Osh01). However, there is no formal, qualitative definition for the Fe II strength, which leaves the interpretation open for debate.

It is also important to note that NLS1 are believed to be young AGN (e.g. Grupe 1996; Mathur 2000). They possess smaller black hole masses and higher accretion rates compared to typical Seyfert 1s of similar luminosities. They also appear to have super-solar metallicities, and many objects have high IR fluxes, which could be attributed to rapid and/or intense episodes of star formation.

Five other radio-loud NLS1 are known, which have more secure confirmation of the NLS1 characteristics: PKS0558–504 (Remillard et al. 1986), RGB J0044+142 (Siebert et al. 1999; though the radio-loudness of this object is questionable, Maccarone et al. 2005), RXJ0134–4258 (Grupe et al. 2000), SDSS J094857.3+002225 (Zhou et al. 2003; Doi et al. 2006), and SDSS J172206.03+565451.6 (Komossa et al. 2006a). Whalen et al. (2006) have recently identified 16 new radio-loud NLS1, but radio spectra are not yet available.

For five of the above mentioned objects (including PKS 2004–447) the radio spectra reveal that all but PKS0558–504 are consistent with the CSS or GPS definition. This is of interest for three reasons. Firstly, NLS1 objects as a class lie on one extreme end of “eigenvector 1” – the anti-correlation between [O III] and Fe II strength (Boroson & Green 1992; see also Brandt & Boller 1997). NLS1 show the most extreme Fe II emission and weakest [O III], while radio-loud objects form the other extreme. Optically selected samples of NLS1 are notoriously radio-quiet (e.g. Greene et al. 2006). Secondly, NLS1 are considered to be in the early stages of AGN evolution (Grupe 1996; Mathur 2000), as are GPS/CSS sources. Though based on very different arguments, the connection between GPS/CSS and NLS1, and AGN evolution is intriguing. Finally, while CSS and GPS sources make up a considerable fraction of radio selected samples (~ 30 and ~ 10 per cent, respectively), the fraction may be significantly higher when considering radio-loud NLS1.

In this work we scrutinise the CSS/NLS1 source PKS 2004–447 across the SED using simultaneous X-ray, near-UV, optical, near-IR, and radio data obtained 2004 April 11–12, with the intention of understanding the connection between CSS and NLS1 sources. The rest of the paper is organised as follows. The observa-

tions and data reduction are described in Section 2. Analysis of the radio, and X-ray data are presented in Section 3, and 4, respectively. The SED of PKS 2004–447 is considered in Section 5. Discussion and summary follow in Section 6 and 7, respectively.

2 OBSERVATIONS AND DATA REDUCTION

A value for the Galactic column density toward PKS 2004–447 of $3.52 \times 10^{20} \text{ cm}^{-2}$ (Dickey & Lockman 1990) is adopted in all of the spectral fits. K-corrected luminosities are calculated using a Hubble constant of $H_0=70 \text{ km s}^{-1} \text{ Mpc}^{-1}$ and a standard flat cosmology with $\Omega_M = 0.3$ and $\Omega_\Lambda = 0.7$. The redshift of PKS 2004–447 is $z = 0.24$ (Drinkwater et al. 1997) and the corresponding luminosity distance is 1.2 Gpc.

2.1 X-ray and UV observations

PKS 2004–447 was observed with *XMM-Newton* (Jansen et al. 2001) for approximately 40 ks between 2004 April 11–12 (revolution 795; obsid 0200360201). During this time all on-board instruments functioned normally. The EPIC pn (Strüder et al. 2001) and MOS (MOS1 and MOS2; Turner et al. 2001) cameras were operated in full-frame mode with the medium filter in place. The Reflection Grating Spectrometers (RGS1 and RGS2; den Herder et al. 2001) also collected data during this time, as did the Optical Monitor (OM; Mason et al. 2001). Due to the low count rate, the RGS data were mostly background dominated and will not be discussed further.

The Observation Data Files (ODFs) were processed to produce calibrated event lists using the *XMM-Newton* Science Analysis System (XMM-SAS v6.5.0) and the most recent calibration files. Unwanted hot, dead, or flickering pixels were removed as were events due to electronic noise. Event energies were corrected for charge-transfer losses, and time-dependent EPIC response matrices were generated using the SAS tasks ARFGEN and RMFGEN. Light curves were extracted from these event lists to search for periods of high background flaring, which were subsequently removed. The total resulting exposures were 33522, 40375 and 40758 s for the pn, MOS1 and MOS2, respectively.

The source plus background photons were extracted from a circular region with a radius of $35''$, and the background was selected from an off-source region with a radius of $50''$ and appropriately scaled to the source region. Single and double events were selected for the pn spectra, and single-quadruple events were selected for the MOS. The spectra were source dominated between 0.3 – 10 keV with a total of 12239 and 8675 source counts collected by the pn and MOS instruments, respectively. Pile-up was negligible in all instruments.

The OM operated in imaging mode, collecting data in *U* (3000 – 3900 Å), *B* (3900 – 4900 Å), *UVW1* (2450 – 3200 Å), *UVM2* (2050 – 2450 Å) and *UVW2* (1800 – 2250 Å). Measured count rates in each filter were converted to flux densities following Chen (2004). Fluxes are given for each OM filter in Table 1.

2.2 ATCA radio observations

The source was observed with the Australia Telescope Compact Array (ATCA) at 1.4, 2.4, 4.8, 4.9, 5.1, 8.6, 17.7, 17.9 GHz on 2004 April 12–13 in the ‘snapshot’ mode, for a total of 4 hours. The observations were performed with a total bandwidth of 128 MHz

Table 1. *XMM-Newton* Optical Monitor observations of PKS 2004–447. Filters and corresponding wavelengths are given in columns 1 and 2, respectively. The flux density in each filter is reported in column 3.

(1) OM Filter	(2) λ (Å)	(3) Flux density ($\times 10^{-16} \text{ erg s}^{-1} \text{ cm}^{-2} \text{ \AA}^{-1}$)
<i>UVW2</i>	2025	12.6 ± 0.5
<i>UVM2</i>	2250	1.62 ± 0.22
<i>UVW1</i>	2825	1.19 ± 0.09
<i>U</i>	3500	1.36 ± 0.06
<i>B</i>	4450	1.44 ± 0.06

Table 2. ATCA radio observations of PKS 2004–447. Frequencies (ν) and corresponding flux densities (f_ν) are given in columns 1 and 2, respectively.

(1) Observed frequency (GHz)	(2) Flux density (mJy)
1.380	791 ± 28
2.372	705 ± 12
4.796	486 ± 34
4.924	469 ± 15
5.052	446 ± 15
8.636	333 ± 13
17.732	230 ± 10
17.861	225 ± 9

using the EW367 array configuration. The source was observed using 8 different frequency settings, each time simultaneously at 2 frequencies.

The detected visibilities were calibrated, flagged and imaged using the MIRIAD data reduction package. Flux density and band-pass calibration were carried out using PKS B1934–638, and the same source was also used to correct for changes in gain and phase.

We used MIRIAD task INVERT to produce images, using uniform weighting to suppress side-lobes but without significantly degrading the beam size (sup=1, robust=0.5 in INVERT). The produced dirty maps were then CLEANed and restored. The MIRIAD task IMFIT was used to determine the integrated flux densities at each frequency, and the results are shown in Table 2.

2.3 Ceduna radio monitoring campaign

The University of Tasmania 30 m Ceduna radio telescope was used to intensively monitor the flux density of the source at 6.65 GHz over the period 2004 February 5 - July 20. During this period PKS 2004–447 was included in the list of sources observed as part of the COSMIC project to monitor intraday variability (McCulloch et al. 2005). The observations were made with a receiver with two orthogonal circular polarizations operating in the frequency range 6.4 – 6.9 GHz with a system equivalent flux density of approximately 550 Jy. The COSMIC project alternates (with a typical period of 10 – 14 days) between monitoring two different groups of sources, one to the north of the zenith at Ceduna, the other to the south. PKS 2004–447 was included in the southern source

Table 3. Siding Spring optical and near infrared observations of PKS 2004–447. Filters and corresponding wavelengths are given in columns 1 and 2, respectively. Flux densities in each filter for nights 1, 2, and 3, are reported in column 3, 4, and 5, respectively. Night 2 (April 11) is quasi-simultaneous with the *XMM-Newton* and ATCA observations.

(1) Filter	(2) λ (Å)	(3) Night 1 ($\times 10^{-16}$ erg s $^{-1}$ cm $^{-2}$ Å $^{-1}$)	(4) Night 2	(5) Night 3
<i>B</i>	4400	1.13 ± 0.51	1.29 ± 0.28	2.09 ± 0.22
<i>V</i>	5500	1.61 ± 0.19	1.63 ± 0.16	1.67 ± 0.11
<i>R</i>	7000	1.38 ± 0.27	1.50 ± 0.17	1.67 ± 0.20
<i>I</i>	8800	0.72 ± 0.10	0.78 ± 0.09	0.87 ± 0.13
<i>J</i>	12390	—	1.24 ± 0.23	—
<i>H</i>	16490	—	0.77 ± 0.13	—
<i>K</i>	21320	—	1.08 ± 0.04	—

list and was observed 30 or more times every day at regular intervals when above an elevation of 10°. The amplitude scale of the observations were set through regular observations of the calibrator PKS B1934–638 which was assumed to have a flux density of 3.92 Jy at 6.65 GHz. The RMS measurement error in a single flux density measurement for COSMIC observations of a source with a mean flux density of 400 mJy is approximately 35 mJy (McCulloch et al. 2005).

2.4 Siding Spring optical and NIR observations

PKS 2004–447 was observed with the Australian National University (ANU) 1-metre telescope at Siding Spring Observatory on the nights of April 10–12 inclusive. The source rose in the middle of the night, and was followed from $\approx 14:30$ UT until twilight – a period of approximately five hours each night.

Observations were all 300 s in length, and were reduced using standard techniques (bias-subtraction, bad-pixel removal and flat-field correction). Photometry of the source was measured in *BVRI* bands, and referenced to the standard stars of Graham (1982) (using those in the E8 region, only ~ 20 arcsec away from the source). The photometry is listed in Table 3. There is some night-to-night variation, particularly in *B* and *I* bands, although comparison with field stars suggests at least some of this variation may be due to changes in the atmospheric transmission rather than intrinsic to the source.

Observations were also made in the near-infrared at *JHK* bands, using the *CASPIR* instrument (McGregor et al. 1994) on the ANU 2.3 m telescope, on the night of the multiwavelength observations (April 11). Images were made from four multiple dithered 60s exposures, each made up of 2×30 s exposures in *J*, 6×10 s exposures in *H*, and 12×5 s exposures in *K*, and were again reduced with standard techniques (e.g. see Whiting et al. 2002).

As well as obtaining the photometry on each night, we tracked the source with sequential *R*-band images (of 300 sec exposure), to search for the presence of rapid variability. Relative photometry was performed using several nearby field stars, but no significant variations of PKS 2004–447 were seen at the precision attained.

2.5 Mt Canopus optical observations

The optical counterpart of PKS 2004–447 was observed with the Mt Canopus 1-m telescope on 3 nights, 2004 April 3, 11 and 12.

Table 4. Mt Canopus optical *B* filter observations of PKS 2004–447 on 2004 April 3, 11 and 12. In the absence of any measurements of standard stars, an offset was applied to equate the magnitude measured on 2005 April 11 to the calibrated magnitude measured at the AAT on the same night. Date and magnitude is given in column 1 and 2, respectively.

(1) Date	(2) <i>B</i>
April 3	19.42 ± 0.03
April 11	19.22 ± 0.04
April 12	19.07 ± 0.03

Measurements were made using an SITE backside thinned 512x512 pixel CCD with Cousins *B* filter. Magnitudes were determined relative to 3 stable reference stars in the CCD field. In the absence of any measurements of standard stars we applied an offset to equate the magnitude measured on 2005 April 11 to the calibrated magnitude measured at the AAT on the same night (see Table 4).

The source increased in brightness by 0.2 magnitudes between the first and second measurements and by a further 0.15 magnitudes on the third measurement. These changes are highly significant statistically. A similar trend is also apparent in the AAT measurements from April 11–12.

3 RADIO ANALYSIS

3.1 Spectral analysis

ATCA pointings were obtained at 1.4, 2.4, 4.8, 4.9, 5.1, 8.6, 17.7 and 17.9 GHz. A power law fit to the spectrum produced a spectral slope of $\alpha = 0.52$. Flux densities are given in Table 2. Calculating the radio loudness ($R = f_{4.9\text{GHz}}/f_B$, Kellerman et al. 1989) from simultaneous optical and radio data resulted in $R = 3800$ confirming the high radio-loudness of this object.

3.2 Radio variability

For the majority of the nearly six month period (2004 February 5 - July 20) that Ceduna monitored PKS 2004–447 the source exhibited relatively little variability; however, in the period just prior to the *XMM-Newton* monitoring significant variations were observed at radio wavelengths. Over a period of 19 days between 2004 March 10–29 (day 68–87 of year 2004) the flux density at 6.65 GHz increased by approximately one-third, from 420 ± 30 mJy to 570 ± 30 mJy (Figure 1). If we assume that the observed variation is intrinsic to the source (rather than due to a propagation effect such as interstellar scintillation), then causality limits the linear size of the varying component to be $c \times t_{\text{obs}}(1+z)$. So for timescale of 19 days in a source at a redshift of 0.24 the linear size of the variable component in the source frame is less than 6.1×10^{11} km (0.02 pc). We emphasize that the size of the entire radio emitting region is likely on pc scales. With our adopted cosmology, the luminosity distance for PKS 2004–447 is 1.2×10^9 pc which requires the angular size of the variable component to be less than $3.4 \mu\text{s}$ (micro-arcseconds). This implies that the brightness temperature of the variable component in the source frame is $1.9 \pm 0.5 \times 10^{14}$ K, well in excess of the inverse Compton limit of 10^{12} K (Kellermann & Pauliny-Toth 1969). There are two possibilities that can account

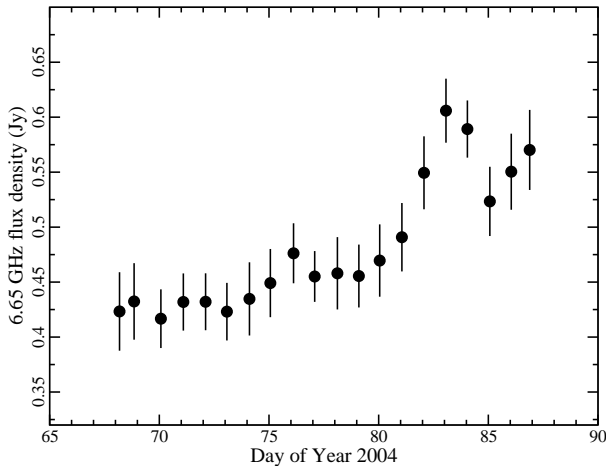


Figure 1. A segment of the 6.65 GHz light curve from the Ceduna monitoring campaign of PKS 2004–447, which lasted nearly six months. The section is of the most variable interval between days 68 – 87.

for this, one is that the jet has a Doppler boosting factor of approximately 6 which reduces observed brightness temperature to around the inverse Compton limit. Alternatively, since the Ceduna and ATCA observations show that approximately 10 days later the radio flux density of the source had returned to its long-term mean value of around 450 mJy, it may be that the component dissipated over that period due to inverse Compton scattering.

The argument above assumes that the observed radio variations are due to intrinsic changes in the source. However, an angular size of the order of a few microarcseconds for the variable component is sufficiently small that we would expect it to show interstellar scintillation (e.g. Bignall et al. 2003). In general the Ceduna light curve over the period in question shows a steady increase in the flux density of the source, however, there is a sudden change around day 81 of year 2004. If intrinsic, this change of around 100 mJy on a timescale of about 3 days implies brightness temperatures of around 10^{15} K, alternatively, it may be that this variation is in fact due to scintillation of the component responsible for the 19-day timescale change.

Although we monitored PKS 2004–447 for approximately half a year, significant variability was only detected over a short period. CSS/GPS sources are typically not Doppler boosted, but there are examples to the contrary (e.g. O’Dea 1998; Aller et al. 2002; Stanghellini et al. 2005). To our knowledge, ours was one of the most intense monitoring campaigns of a CSS source, so it is difficult to determine if the behaviour exhibited by PKS 2004–447 is characteristic of CSS sources. In any regard, our campaign shows that daily radio frequency monitoring of such sources from programmes such as COSMIC (McCulloch et al. 2005) can reveal phenomena that are likely to be missed by more traditional monitoring where the interval between observations is weeks or months.

4 X-RAY SPECTRAL AND TIMING ANALYSIS

4.1 Spectral analysis

We began the X-ray spectral analysis by fitting the observed 2 – 10 keV spectrum of each EPIC instrument with a single power law. Finding relatively good agreement within the uncertainties we pro-

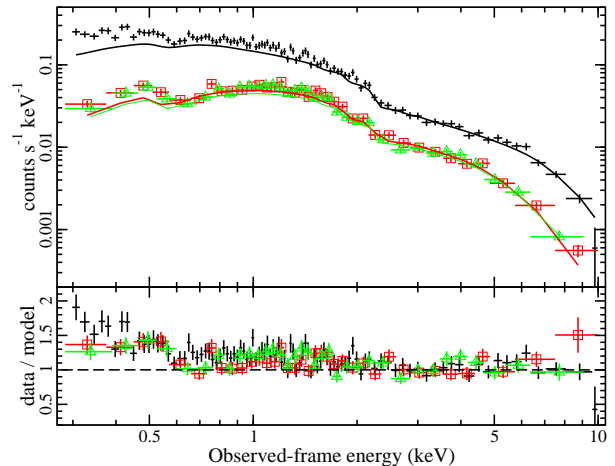


Figure 2. A common power law ($\Gamma = 1.44 \pm 0.06$) fitted to the observed 2–10 keV pn (black crosses), MOS1 (red squares) and MOS2 (green triangles) spectra. The residuals from extrapolating this fit to 0.3 keV are shown in the lower panel, and indicate possible soft excess emission. However, a single power law fit to the entire spectrum is statistically satisfactory.

ceeded by fitting the three spectra together. The power law fit to the 2 – 10 keV EPIC spectrum resulted in a good fit ($\chi^2_{\nu}/\text{dof} = 0.84/306$) with a photon index of $\Gamma = 1.44 \pm 0.06$.

Extrapolating this power law to 0.3 keV revealed an excess forming toward lower energies (Figure 2). Even though refitting a single power law to the 0.3 – 10 keV spectrum ($\Gamma = 1.56 \pm 0.02$) resulted in an acceptable fit ($\chi^2_{\nu}/\text{dof} = 0.97/792$) positive residuals remained below ~ 0.6 keV.

Replacing the single power law with a broken power law provided significant improvement ($\Delta\chi^2 = 35$ for 2 additional free parameters) with an F-test probability of $\sim 10^{-8}$. In this case the high-energy and low-energy power laws had $\Gamma = 1.52 \pm 0.02$ and $\Gamma = 2.10^{+0.23}_{-0.19}$, respectively, with the break occurring at $E_b = 613^{+79}_{-59}$ eV.

Additional neutral absorption at the redshift of PKS 2004–447 was considered in all of the attempted models, but not found to be required. The 90 per-cent upper limit on the column density of any such absorber is $< 1.6 \times 10^{19} \text{ cm}^{-2}$. The existence of an emission feature at FeK α energies, which could arise from a putative torus or accretion disc was also examined. Again, considering such a feature did not significantly improve existing fits. The 90 per-cent upper limit on the equivalent width of a narrow emission line between 6.4 – 7.0 keV was $EW < 54$ eV.

The X-ray spectrum of PKS 2004–447 is unusually flat for a NLS1, but not unlike radio-loud AGN. There is a slight indication of a weak soft excess below ~ 1 keV, which is typical of NLS1, but also comparable to the broken power law seen in Flat-Spectrum Radio Quasar (FSRQ) and Low-energy-peaked BL Lacs. On the other hand, X-ray spectral studies of samples of GPS sources (Guainazzi et al. 2006 and Vink et al. 2006) do not show evidence of soft excess emission. We note that statistically a single power law provides a satisfactory fit, and that higher quality data are required to pin down the existence of soft excess emission in PKS 2004–447.

From the broken power law fit to the EPIC data, an unabsorbed 0.3–10 keV flux of $\sim 1.5 \times 10^{-12} \text{ erg cm}^{-2} \text{ s}^{-1}$ is estimated. The intrinsic 0.3–10 keV and 2–10 keV luminosities are 2.42×10^{44} and $1.54 \times 10^{44} \text{ erg s}^{-1}$, respectively.

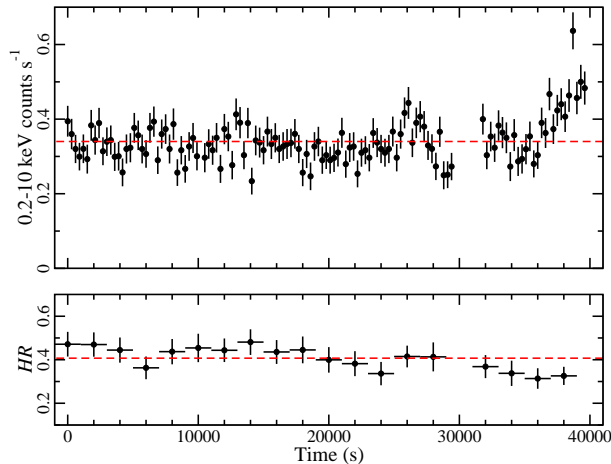


Figure 3. Top panel: The EPIC pn 0.2 – 10 keV light curve (300 s bins). Lower panel: The hardness ratio ($HR = H - S/H + S$, where $H = 0.7 - 10$ keV and $S = 0.2 - 0.7$ keV) variability curve (2000 s bins). The energy bands were selected to examine the possible different components predicted by the broken power law model (Section 4.1). In both figures, the dashed lines mark the average values. Variability is negligible in the light curve with the exception of the final 4 ks when a 30 per cent flux increase is seen. Though not highly significant ($\chi^2_\nu = 1.05$), the HR shows softening over the course of the observation.

4.2 X-ray variability

4.2.1 Short-term X-ray variability

Short-term flux variations were examined over the 40 ks *XMM-Newton* observation of PKS 2004–447. The 0.2 – 10 keV light curve (Figure 3, upper panel) shows some variability ($\chi^2_\nu/\text{dof} = 1.95/124$), most of it appearing as a 30 per cent rise in count rate during the final ~ 4 ks.

Spectral variations with time were searched for by constructing a hardness ratio ($HR = H - S/H + S$, where $H = 0.7 - 10$ keV and $S = 0.2 - 0.7$ keV) variability curve (Figure 3, lower panel). The energy bands were selected to examine the potentially components on either side of the break energy predicted by the broken power law model (Section 4.1). The hardness ratio curve is not highly variable when compared to a constant fit ($\chi^2_\nu = 1.05$), but there is a softening trend over the course of the observation. Therefore, it does seem plausible that multiple components may be present in the X-ray continuum.

4.2.2 Long-term X-ray variability

The only other X-ray observation of PKS 2004–447 was a detection during the *ROSAT* All-Sky Survey (RASS; Voges et al. 1999). At that time it was detected as a faint source with a 0.1 – 2.4 keV count rate of $2.2 \pm 1.1 \times 10^{-2}$ count s^{-1} (Siebert et al. 1998). Assuming a photon index in this energy band of either 2.10 or 1.56 (as derived from our broken power law and power law fits in Section 4.1), the unabsorbed 0.3 – 2.4 keV flux is 2.0 ± 1.0 or $2.5 \pm 1.2 \times 10^{-13}$ erg cm^{-2} s^{-1} , respectively. In this same energy band, the *XMM-Newton* flux is $6.09^{+0.89}_{-1.06} \times 10^{-13}$ erg cm^{-2} s^{-1} . This indicates that, at the very least, modest X-ray variability on about the 30 per cent level occurs on yearly time scales. This level of variability is comparable with the centimetre fluctuations on similar time scales seen in PKS 2004–447.

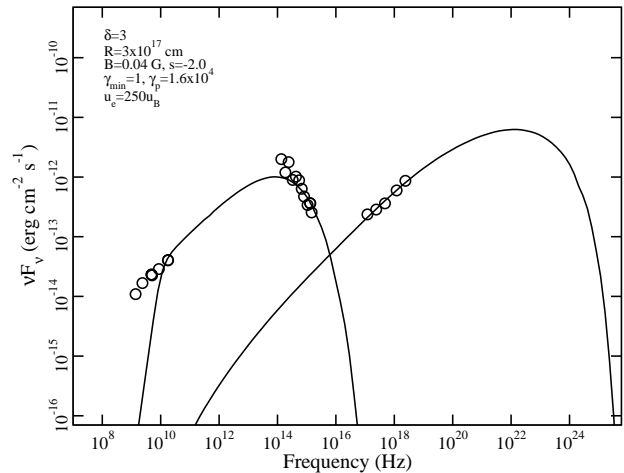


Figure 4. Synchrotron/SSC scenario applied to the SED of PKS 2004–447. Model parameters are given in the top left. For simplicity the X-ray data are shown as five points between 0.3 – 10 keV. See text for details.

5 CONTEMPORANEOUS SPECTRAL ENERGY DISTRIBUTION

We considered the possibility that the SED of PKS 2004–447 is generated by synchrotron plus synchrotron self-Compton (SSC) processes. Such models are reasonably successful in describing the SED of blazars and even some un-beamed radio galaxies (e.g. Chiaberge et al. 2001). The adopted model (Kataoka et al. 1999) assumes a single zone homogeneous SSC in a spherical volume, which is probably an oversimplification, but allows the source to be modelled in a self-consistent way with a minimum of parameters, and is not unreasonable given the compactness of PKS 2004–447. Given the modest radio variability (Sect 3.2), models with large Doppler beaming factors are not considered. The model shown in Figure 4 reproduces the general trend of the SED quite well; however it significantly under estimates the radio emission. Such discrepancies in the radio are found in many studies and it is believed to be a consequence of the radio emission originating from a much larger region than the X-rays and gamma-rays. Even so, the current region size ($R \approx 0.1$ pc) is too large to account for the short-term X-ray variability (Sect. 4.2). Furthermore, explaining the high X-ray brightness would require a large electron-to-magnetic energy density ratio (u_e/u_B) for the SSC component. In extreme objects such as blazars, the ratio is typically less than 100, whereas for all the X-ray emission to be produced by the single zone SSC model in PKS 2004–447 the ratio would have to be about 250.

We have examined whether the SED can be constrained by data at higher energies. Mattox et al. (2001) made a quantitative evaluation of potential radio identifications for 3EG EGRET sources based on the 5 GHz flux density, spectral index, and proximity to the EGRET source of candidate counterparts. PKS 2004–447 was considered as a counterpart to the unidentified EGRET source 3EG J1958–4443, however the association had a posteriori probability of less than 2×10^{-4} and so was considered unlikely (although no more likely candidates were found). Even considering the SED model with a very high u_e/u_B , the predicted 10^{23} Hz flux density falls below the detection sensitivity of EGRET.

A synchrotron/SSC model, which adopts a much larger emitting region characterises the radio-to-UV emission quite well (Figure 5). On the other hand, assuming equipartition conditions or

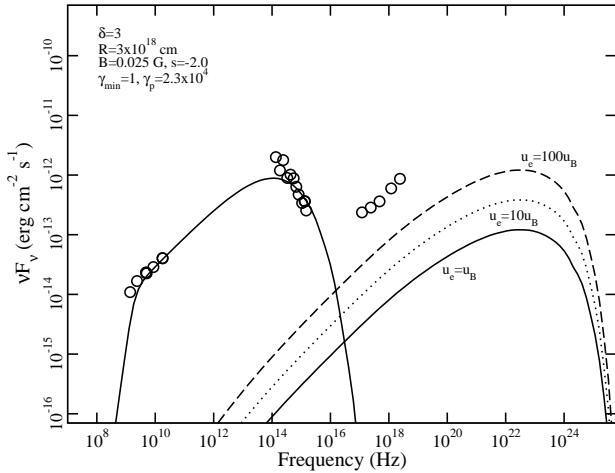


Figure 5. Synchrotron/SSC scenario applied to the SED of PKS 2004–447. The emitting region is much larger than in Figure 4, which better describes the radio emission. The SSC is described with more typical values of u_e/u_B . In this case, a component in addition to SSC is required to fit the high X-ray brightness.

moderate particle-dominated parameters, the SSC model under estimates the observed X-ray emission by an order of magnitude (Figure 5). This may not be unreasonable if the SED is a combination of jet emission and disc/halo emission as typically seen in Seyfert 1s. Indeed the short term X-ray variability is consistent with originating from a much smaller region than most of the radio emission.

We probe this further by re-examining the *XMM-Newton* X-ray data. The data are refitted with a thermal Comptonisation model (Titarchuk 1994) plus an underlying power law to mimic the SSC component. The photon index of the SSC power law is fixed to $\Gamma = 1.52$ (similar to the slope of the radio spectrum), while the normalisation is allowed to vary freely. This produces a good fit ($\chi^2_{\nu}/\text{dof} = 0.97/790$) similar to the broken power law model in Section 4.1. The model parameters: plasma temperature ($T_e \approx 54$ keV), optical depth ($\tau \approx 1.12$) and seed photon temperature ($kT = 66 \pm 17$ eV) are not inconsistent with physical conditions expected in AGN where the seed photons provided by the accretion disc are up-scattered to higher energies by the hot electron corona. Of course, the values are uncertain given the known degeneracy between T_e and τ . In this interpretation the flux density of the underlying power law is $1.2 \pm 0.4 \times 10^{-14}$ erg cm $^{-2}$ s $^{-1}$ keV $^{-1}$ at 2 keV, consistent with originating from the SSC component with $u_e \approx 10u_B$ (Figure 6).

A second issue is the slight excess seen in the infrared data compared to the synchrotron models shown in Figures 4 and 5. de Vries et al. (1998) recognised this IR excess in other CSS sources and attributed it to a ~ 1000 K blackbody arising from an AGN heated torus. We draw a similar conclusion for the IR emission in PKS 2004–447, which can be fitted by a blackbody with a temperature of about 1000 – 1500 K (Figure 6).

Overall, the inclusion of these additional component to the synchrotron/SSC continuum provides a reasonable approximation of the SED of PKS 2004–447 (solid line in Figure 6).

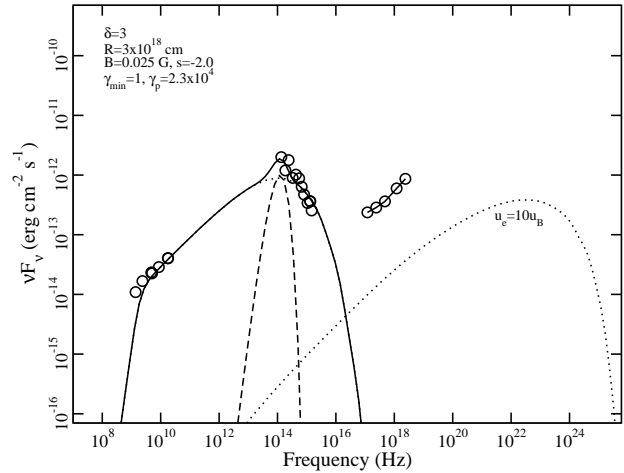


Figure 6. A possible interpretation for the SED of PKS 2004–447 (black solid line is the sum of all components). Most of the underlying continuum is produced by the synchrotron/SSC mechanism (dotted line). The IR excess is attributed to 1000 – 1500 K blackbody emission from the AGN heated torus (dashed line). The strong X-ray excess is generated by thermal Comptonisation processes close to the central black hole.

6 DISCUSSION

6.1 The SED of PKS 2004–447

The shape of the SED of PKS 2004–447 portrays the typical double-hump form that is often seen in radio-loud, blazar-type AGN. The single zone homogeneous synchrotron/SSC interpretation appears to be a good base model. However, the fact that the normally constant, long-term radio light curve shows occasional activity and because the X-ray emission is apparently excessive, indicate that a single zone model is probably an oversimplification.

6.1.1 General SED characteristics

Utilising the simultaneous UV data we calculated the optical-to-X-ray spectral slope (α_{ox}) of PKS 2004–447 to be approximately -0.95 . Considering the UV luminosity dependence of α_{ox} for radio-quiet, unabsorbed AGN (e.g. NLS1) a value of $\alpha_{ox} = -1.27$ is predicted (Strateva et al. 2005) indicating that the spectral slope of PKS 2004–447 is flat compared to NLS1-type objects.

We also calculated the spectral slopes between the radio and optical (α_{ro}), and radio and X-rays (α_{rx}) as shown by Padovani et al. (2002) for a sample of blazar-type objects. In comparing the values of all the spectral indices measured for PKS 2004–447 to the Padovani sample, it is found that the characteristics of PKS 2004–447 are very similar to FSRQ. Essentially, PKS 2004–447 resembles a radio-loud quasar, but with several atypical properties (e.g. IR excess but no intrinsic X-ray absorption, normally low radio and X-ray variability, NLS1 classification), and from the SED modelling the only way to recover a typical blazar SED is with a very large u_e/u_B .

6.1.2 The X-ray excess

As seen in Figures 4 and 5 simple synchrotron/SSC models are unable to simultaneously fit the radio and X-ray emission. The shortcoming is apparently the difficulty in fitting the “too bright” X-ray

emission in PKS 2004–447. The high X-ray brightness could be explained by a large $u_e/u_B \approx 250$. However, this is quite unusual compared to other types of jet-dominated objects.

Alternatively, the X-ray emission could require an additional component, which originates close to the black hole. The presence of some short-term X-ray variability and normally constant radio variability implies that the X-ray emitting region is probably much smaller than the radio one. The SED of PKS 2004–447 is well approximated if in addition to a synchrotron/SSC continuum, the model takes on a Comptonisation component to describe the strong X-ray emission (empirically, a single or broken power law fit the X-rays adequately). In this case, the derived model parameters are not atypical of expected physical conditions in AGN.

6.1.3 Excess optical reddening

Excess emission in the IR has been seen in other CSS sources (de Vries et al. 1998); therefore its presence in PKS 2004–447 is not unexpected. This excess can be fit with a 1000 – 1500 K blackbody, which is consistent with originating in an AGN heated torus, but notably also close to the sublimation temperature of dust. The host galaxy cannot be excluded for contributing to this component. However, the optical spectra shown in Osh01 do not exhibit any striking galactic features, so we consider it unlikely that the host galaxy dominates this spectral region.

The absence of big blue bump emission at UV energies could imply reddening of the optical spectrum by this component. The Balmer decrement ($H\alpha/H\beta$) was measured in PKS 2004–447 using the low-resolution optical spectrum shown in figure 2 of Osh01. The ratio was $H\alpha/H\beta \approx 6$ for the narrow-line region (NLR) lines, with considerable uncertainty arising from the difficulty in isolating the narrow component from the broad component in the fit (~ 60 per cent). Assuming that the narrow Balmer lines are due to case B recombination then by following the example of Veilleux et al. (1999), and using the parameterised reddening curve for our Galaxy (Miller & Mathews 1972) the amount of intrinsic extinction in the NLR of PKS 2004–447 can be estimated. If the ratio of total to selective extinction is 3.1 then the visible extinction in PKS 2004–447 is $A_V = 1.9 \pm 1.5$. Even within the large range of uncertainty the extinction is significantly higher than the estimated intrinsic column density found in the X-ray spectral fits ($N_H < 1.6 \times 10^{19} \text{ cm}^{-2}$). Following Predehl & Schmitt (1995), the X-ray measurements give $A_V < 0.01$.

The discrepancy could be understood if PKS 2004–447 had a very different gas-to-dust ratio than our Galaxy. This could perhaps be achieved as the radio jet, which likely terminates on NLR-scales in PKS 2004–447, deposits material from the nucleus into the NLR. It would be of interest to examine this issue in other CSS/GPS sources to determine if the discrepancy in X-ray and optically measured A_V is a class property.

6.2 PKS 2004–447: NLS1, CSS, or both?

The radio properties of PKS 2004–447 satisfy the CSS definition of the source. However, the optical spectral properties are not entirely consistent with the general behaviour of CSS sources (e.g. Gelderman & Whittle 1994, Morganti et al. 1997). Osh01 proposed a NLS1 classification for PKS 2004–447 because of its relatively weak [O III] emission and narrow $H\beta$ line. The classification has prompted some debate primarily due to the lack of strong Fe II emission in PKS 2004–447, and it has been suggested that

PKS 2004–447 is probably a type 2 AGN (e.g. Sulentic et al. 2003, Zhou et al. 2003). However, the X-ray emission is unabsorbed, and there is evidence for short-term variability and a weak soft excess. Moreover, the [O III] emission is relatively weak and the $H\beta$ emission is variable on at least yearly time scales (Osh01) indicating that the broad-line region is probably visible. For the sake of argument, in this discussion we will treat PKS 2004–447 as a NLS1.

As such, there are four rather securely identified radio-loud NLS1 and perhaps two more questionable objects (PKS 2004–447 and RGB J0044+193), which have been relatively well examined. Nonetheless, of particular interest is that five of these six objects display steep or inverted radio spectra, which are consistent with radio definitions of CSS/GPS sources. This coincidence in definitions presents a challenging area of research, for a number of reasons. First, radio-loud AGN and NLS1 occupy distinctly different regions of the primary eigenvector 1 parameter space (Boroson & Green). NLS1 are typically very radio-quiet. Secondly, the fraction of radio-loud NLS1 which are CSS/GPS sources (5/6) is potentially much higher than the fraction of CSS/GPS sources in radio selected sample (10 – 30 per cent). Thirdly, both classes of objects are believed to be in the early stages of AGN evolution. This implies that radio-loud NLS1 could be CSS/GPS sources, perhaps in a situation where the black hole environment and the radio component are forming simultaneously.

We compared some of the NLS1-CSS/GPS sources mentioned above with X-ray samples of GPS objects (from Vink et al. 2006 and Guainazzi et al. 2006) to determine how similar the two groups appear. Our findings are illustrated in Figure 7 and 8 where the NLS1-CSS/GPS objects (PKS 2004–447, RXJ0134–4258, RGB J0044+193) are shown as filled squares (a common cosmology is adopted for the figures).

In Figure 7 we note that the NLS1-CSS/GPS objects appear to have stronger X-ray emission compared to the radio emission than typical GPS sources, which are known to be X-ray weak. This is in line with the additional X-ray component required to fit the SED of PKS 2004–447. The significant, rapid X-ray variability seen in the three objects (see Grupe et al. for RXJ0134–4258 and Siebert et al. for RGB J0044+193) indicate that, like PKS 2004–447, the X-ray emission region is not extended.

In Figure 8 a comparison is made between the amount of intrinsic absorption seen in NLS1-CSS/GPS and the GPS sample. There is support that lower intrinsic absorption is seen in the NLS1-CSS/GPS, independent of X-ray luminosity.

Significant statements cannot be made given the small samples presented in Figure 7 and 8; however, there is an indication that NLS1-CSS/GPS and ‘typical’ GPS sources differ in X-ray behaviour.

7 SUMMARY

An investigation of the SED of PKS 2004–447, a CSS and possible radio-loud NLS1, is presented, utilising contemporaneous X-ray, near-UV, optical, near-IR, and radio data. The main results are summarised here.

- The SED cannot be fitted by a single zone homogeneous SSC model. Primarily, the difficulty is in simultaneously fitting the radio and excessive X-ray emission. Models in which a second component (probably arising from Comptonisation of accretion disc photons) is adopted to describe the X-ray emission or SSC models that require very high values of u_e/u_B seem plausible.

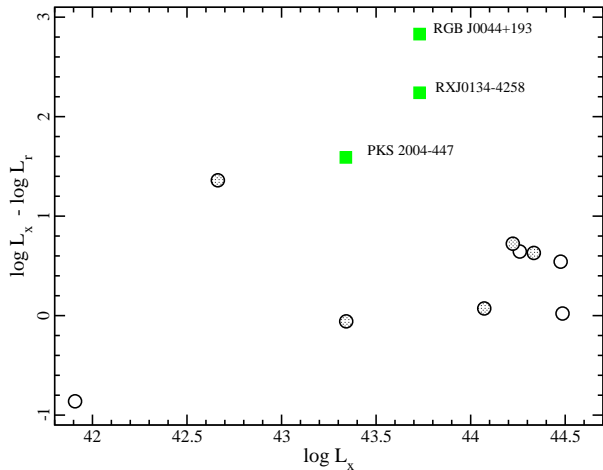


Figure 7. The 2 – 10 keV and 5 GHz luminosity ratio plotted against 2 – 10 keV luminosity (erg s^{-1}). The circles represent the GPS samples of Guainazzi et al. (2006; empty circles) and Vink et al. (2006; shaded circles). The green, filled squares represent the radio-loud NLS1-CSS/GPS objects, which are also designated as GPS/CSS sources. There is possible indication that the NLS1-CSS/GPS are not X-ray weak like typical GPS sources. The luminosity of PKS 2004–447 appears different in the figure than in the text because the cosmology was changed to match the luminosities of the larger surveys.

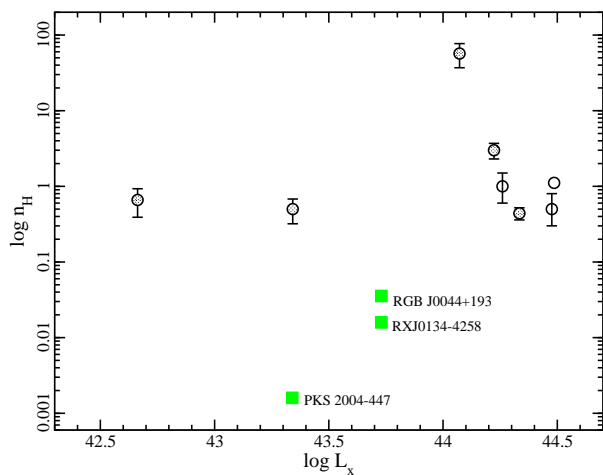


Figure 8. Intrinsic neutral hydrogen column density as a function of 2 – 10 keV luminosity (erg s^{-1}). The symbols are as in Figure 7. Symbols without error bars in the column density indicate upper limits. There is some indication that the NLS1-CSS/GPS objects possess less absorption at a given X-ray luminosity than the GPS sources. The luminosity of PKS 2004–447 appears different in the figure than in the text because the cosmology was changed to match the luminosities of the larger surveys.

- Excess emission is also seen in the SED at IR energies. In fact, the peak emission in the SED appears to be in the IR. This excess can be well fitted with a $T \approx 1000$ K blackbody, likely originating from an AGN heated torus; however we cannot exclude some contribution from the host galaxy. No excess absorption (above Galactic column density) or fluorescent iron line is detected in the X-ray spectrum, as expected if the X-rays transverse a high column

density. Analysis of a non-contemporaneous, low-resolution optical spectrum suggests that the NLR is much more reddened than the X-ray emitting region. This could arise if the gas-to-dust ratio in PKS 2004–447 is very different than in our own Galaxy, but further analysis of higher quality optical spectra are required to draw firm conclusions.

- Long-term radio monitoring of PKS 2004–447 shows a rather constant light curve over a six month period with the exception of one event when the 6.65 GHz flux increases by ~ 35 per cent in 19 days. Interstellar scintillation cannot be excluded as the cause of the variability, but the detection of the rare event demonstrates the potential of intense monitoring campaigns such as COSMIC (McCulloch et al. 2005). No matter whether the outburst has an intrinsic or extrinsic origin, it indicates a small emitting region for at least some of the radio flux.

- There is some indication of a possible connection between NLS1 and CSS/GPS sources. In comparison to other GPS sources, these radio-loud NLS1 seem to exhibit greater X-ray emission relative to radio flux, and lower intrinsic absorption. However, a larger and more uniformly selected sample is required to draw convincing conclusions.

The recent discovery of a large number of radio-loud NLS1 (Whalen et al. 2006, Komossa et al. 2006b) holds many possibilities for future investigations of the potential connection between radio-loud NLS1 and CSS/GPS sources.

ACKNOWLEDGEMENTS

Based on observations obtained with *XMM-Newton*, an ESA science mission with instruments and contributions directly funded by ESA Member States and the USA (NASA). The Australia Telescope Compact Array is part of the Australia Telescope which is funded by the Commonwealth of Australia for operation as a National Facility managed by CSIRO. LCG acknowledges funding from the Japan Society for the Promotion of Science through a JSPS Postdoctoral Fellowship, and would like to thank Patricia Arevalo for helpful discussions. SPE would like to thank the Australian Research Council for financial support for this work, Steve Carter and Cliff Senkbeil for their assistance collecting and processing the data, and Jim Lovell and Giuseppe Cimò for useful discussions about the nature of the Ceduna variability. Thanks to Ivy Wong for assistance with the optical observing, Steve Longmore for taking the near-infrared CASPIR observations, and the anonymous referee for a quick and helpful report.

REFERENCES

- Aller M., Aller H., Hughes P., Plotkin R., 2002, in: *Proc. of the 6th European VLBI Network Symposium*, Ros E., Porcas R., Lobanov A., Zensus J., eds, MPIfR, Bonn, Germany, p131
- Baker J., Hunstead R., Brinkmann W., 1995, *MNRAS*, 277, 553
- Bicknell G. V., Dopita M. A., O’Dea C., 1997, *ApJ*, 485, 112
- Bignall H.E. et al. 2003, *ApJ*, 585, 653
- Boroson T. A., Green R. F., 1992, *ApJS*, 80, 109
- Brandt W. N., Boller Th., 1997, in: *Emission Lines in Active Galaxies: New Methods and Techniques*, Peterson B., Cheng F., Wilson A., eds, ASP Conf. Series Vol. 113, p248
- Chen B., 2004, *XMM-Newton Calibration Documents* (CAL-TN-0019)
- Chiaberge M., Capetti A., Celotti A., 2001, *MNRAS*, 324, 33
- den Herder J. W. et al. 2001, *A&A*, 365, 7

- de Vries W., O'Dea C., Baum S., Perlman E., Lehnert M., Barthel P., 1998, *ApJ*, 503, 156
- de Vries W., O'Dea C., Barthel P., Thompson D., 2000, *A&AS*, 143, 181
- Dickey J. M., Lockman F. J., 1990, *ARA&A*, 28, 215
- Doi A., Nagai H., Asada K., Kamenno S., Wajima K., Inoue M., 2006, submitted to *AJ*
- Drinkwater M. J. et al. 1997, *MNRAS*, 284, 85
- Edwards P. G., Tingay S. J., 2004, *A&A*, 424, 91
- Elvis M., Fiore F., Wilkes B., McDowell J., Bechtold J., 1994, *ApJ*, 422, 60
- Fanti R., Fanti C., Schilizzi R. T., Spencer R. E., Rendong N., Parma P., van Breugel W., Venturi T., 1990, *A&A*, 231, 333
- Gelderman R., Whittle M., 1994, *ApJS*, 91, 491
- Graham J. A., 1982, *PASP*, 94, 244
- Greene J., Ho L., Ulvestad J., 2006, *ApJ*, 636, 56
- Grupe D., 1996, PhD thesis, Univ. Göttingen
- Grupe D., Leighly K. M., Thomas H.-C., Laurent-Muehleisen S. A., 2000, *A&A*, 356, 11
- Goodrich R. W., 1989, *ApJ* 342, 234
- Guainazzi M., Siemiginowska A., Stanghellini C., Grandi P., Piconcelli E., Azubike C., 2006, *A&A*, 446, 87
- Heckman T., O'Dea C., Baum S., Laurikainen E., 1994, *ApJ*, 428, 65
- Jansen F. et al. 2001, *A&A*, 365, L1
- Kataoka J. et al. 1999, *ApJ*, 514, 138
- Kellermann K.I., Pauliny-Toth I.I.K., 1969, *ApJ*, 155, L71
- Kellermann K., Sramek R., Schmidt M., Shaffer D., Green R., 1989, *AJ*, 98, 1195
- Komossa S., Voges W., Adorf H.-M., Xu D., Mathur S., Anderson S., 2006a, *ApJ*, 639, 710
- Komossa S. et al. 2006b, submitted to *AJ* (astro-ph/0603680)
- Labiano A. et al. 2005, *A&A*, 436, 493
- Lovell J. E. J., 1997, PhD thesis, Univ. Tasmania
- Maccarone T. J., Miller-Jones J. C. A., Fender R. P., Pooley G. G., 2005, *A&A*, 433, 531
- Mason K. O. et al. 2001, *A&A*, 365, 36
- Mathur S., 2000, *MNRAS*, 314, 17
- Mattox J. R., Hartman R. C., Reimer O., 2001, *ApJS*, 135, 155
- McCulloch P. M., Ellingsen S. P., Jauncey D. L., Carter S. J. B., Cimò G., Lovell J. E. J., Dodson R. G., 2005, *AJ*, 129, 2034
- McGregor P., Hart J., Downing M., Hoadley D., Bloxham G., 1994, in: *Infrared Astronomy with Arrays, The Next Generation*, McLean I. S., ed, Astrophysics and Space Science Library, Vol. 190, p299
- Miller J., Mathews W., 1972, *ApJ*, 172, 593
- Morganti R., Tadhunter C. N., Dickson R., Shaw M., 1997, *A&A*, 326, 130
- O'Dea C., 1998, *PASP*, 110, 493
- O'Dea C., Baum S., 1997, *AJ*, 113, 148
- Oshlack A., Webster R., Whiting M., 2001, *ApJ*, 558, 578 (Osh01)
- Osterbrock D. E., Pogge R. W., 1985, *ApJ* 297, 166
- Padovani P., Costamante L., Ghisellini G., Giommi P., Perlman E., 2002, *ApJ*, 581, 895
- Predehl P., Schmitt J., 1995, *A&A*, 293, 889
- Preston R. A., Morabito D. D., Williams J. G., Faulkner J., Jauncey D. L., Nicolson G., 1985, *AJ*, 90, 1599
- Remillard R. A., Bradt H. V., Buckley D. A. H., Roberts W., Schwartz D. A., Tuohy I. R., Wood K., 1986, *ApJ*, 301, 742
- Siebert J., Brinkmann W., Drinkwater M. J., Yuan W., Francis P. J., Peterson B. A., Webster R. L., 1998, *MNRAS*, 301, 261
- Siebert J., Leighly K. M., Laurent-Muehleisen S. A., Brinkmann W., Boller Th., Matsuoka M., 1999, *A&A*, 348, 678
- Strüder L. et al. 2001, *A&A*, 365, L18
- Snellen I. A. G., Mack K.-H., Schilizzi R. T., Tschager W., 2003, *PASA*, 20, 38
- Stanghellini C., O'Dea C., Dallacasa D., Cassaro P., Baum S., Fanti R., Fanti C., 2005, *A&A*, 443, 891
- Strateva I., Brandt W., Schneider D., Vanden Berk D., Vignali C., 2005, *AJ*, 130, 387
- Sulentic J., Zamfir S., Marziani P., Bachev R., Calvani M., Dultzin-Hacyan D., 2003, *ApJ*, 597, 17
- Tasker N. J., 2000, PhD thesis, Marquarie Univ.
- Titarchuk L., 1994, *ApJ*, 434, 313
- Turner M. J. L. et al. 2001, *A&A*, 365, 27
- Veilleux S., Kim D., Sanders D., 1999, *ApJ*, 522, 113
- Vink J., Snellen I., Mack K.-H., Schilizzi R., 2006, accepted for publication in *MNRAS* (astro-ph/0601141)
- Voges W. et al. , 1999, *A&A*, 349, 389
- Whalen D. J., Laurent-Muehleisen S. A., Moran E. C., Becker R. H., 2006, accept for publication in *ApJ* (astro-ph/0601162)
- Whiting M., Oshlack A., Webster R., 2002, *PASA*, 19, 222
- Wright A., Otrupcek R., 1990, *PKS Catalog*, 0
- Zhou H-Y, Wang T-G, Dong X-B, Zhou Y-Y, Li C., 2003, *ApJ*, 584, 147

This paper has been typeset from a $\text{\TeX}/\text{\LaTeX}$ file prepared by the author.